Microbial Fuel Cell Performance with a Pressurized Cathode Chamber

JEFFREY J. FORNERO,[†] MIRIAM ROSENBAUM,[†,‡] MICHAEL A. COTTA,[‡] AND LARGUS T. ANGENENT*[,†,§]

Department of Energy, Environmental and Chemical Engineering, Washington University in St. Louis, One Brookings Drive, CB 1180, St. Louis, Missouri 63130, Fermentation Biotechnology Research Unit, United States Department of Agriculture, Agricultural Research Service (ARS), National Center for Agricultural Utilization Research (NCAUR), Peoria, Illinois 61604, and Department of Biological and Environmental Engineering, Cornell University, 214 Riley-Robb Hall, Ithaca, New York 14853

Received June 3, 2008. Revised manuscript received August 15, 2008. Accepted August 25, 2008.

Microbial fuel cell (MFC) power densities are often constrained by the oxygen reduction reaction rate on the cathode electrode. One important factor for this is the normally low solubility of oxygen in the aqueous cathode solution, which creates mass transport limitation and hinders oxygen reduction at the electrocatalyst (platinum, Pt). Here, we increased the air pressure in the cathode chamber to increase the solubility and consequently the availability of oxygen, which is a function of the partial pressure. Under stable anode and cathode conditions, an MFC was tested with an anion-exchange membrane (AEM) and a cation-exchange membrane (CEM) at atmospheric pressure, +17.24 kPa (2.5 psig), and +34.48 kPa (5.0 psig) overpressure of air. The cell potential at an external resistance of 100 Ω increased from 0.423 to 0.553 V by increasing the cathode pressure from atmospheric pressure to 17.24 kPa for an MFC with AEM, and this resulted in a 70% increase in the power density (4.29 vs 7.29 W/m^3). In addition, the MFC produced 66−108% more power with AEM in comparison to CEM under the same operating conditions. We discussed the mechanisms that explain this. Results from this study demonstrate that higher MFC power densities can be realized by increasing the cathode air pressure if the membrane oxygen diffusion to the anode can be controlled.

Introduction

Persistent high energy prices and the desire for environmental sustainability will likely challenge traditional engineering practices that were developed in an era of relatively low energy costs. One such area is conventional secondary treatment of wastewater with activated sludge systems. It was estimated that wastewater treatment consumes ∼1.5% of the total electricity usage in the U.S. and that activated sludge aeration requires ∼50% of that energy (*1*). Microbial fuel cell (MFC) technology holds promise as a viable alternative to secondary activated sludge systems because of the ability to simultaneously treat wastewater and generate electricity (*2*−*5*). Thus, one priority for the development and application of MFC technology is to transform wastewater treatment from an energy-consuming process to a sustainable, energy-neutral or energy-producing, process.

Recently, novel MFC designs have been proposed to further increase their power densities (*3, 6*−*9*). These designs share a common feature of proximate anode and cathode electrodes to reduce the voltage drop associated with the resistance of the flow of ions through the electrolyte (i.e., ohmic losses). Ion transfer between the anode and cathode is necessary to maintain fuel cell electroneutrality because of the movement of negatively charged electrons from the anode to the cathode. To achieve this counterbalance, either negative charge equivalents (anions/hydroxide ions) travel from the cathode to the anode, or positive charge equivalents (cations/protons) move from the anode to the cathode depending on the selection of the ion-exchange membrane material (anion-exchange membrane [AEM] vs cation-exchange membrane [CEM]). Because MFCs operate near neutral pH in the anode and cathode chambers, ions other than hydroxide ions or protons are present at higher concentrations than the hydroxide ions or protons themselves ($\sim10^{-6}$ to $\sim10^{-8}$ M) in wastewater and buffer solutions, respectively. Therefore, the transmembrane transport of nonhydroxide/nonproton ion species is the dominant mechanism to maintain electroneutrality in MFCs (*10*−*12*).

Improvements to the cathode design in MFCs have also led to considerable power density increases. To date, cathode designs have mainly used two different terminal electron acceptors: oxygen and nonsustainable chemicals, such as ferricyanide (*5, 12*). Cathode designs using oxygen as the terminal electron acceptor include cathodes with oxygen reduction catalysts submerged in an electrolyte (i.e., electrolyte cathodes) (*10, 12, 13*), air cathodes with oxygen reduction catalysts (*3, 14, 15*), and biocathodes (*6, 16, 17*). The primary limitation of power densities for oxygen as the electron acceptor results from the activation losses (i.e., voltage losses associated with the electrode electron-transfer reactions) at the (bio)catalyst reaction sites (*18*). Another limitation of oxygen cathodes with respect to the power density, especially for electrolyte cathodes, are the mass transport losses of oxygen to the catalyst reaction sites on the cathode electrode (*10, 14*). The relatively low solubility of oxygen affects the activation and oxygen mass transport losses in the cathode electrolyte. Because the solubility of air and consequent availability of oxygen at the reaction sites are a function of their partial pressure, a pressurized cathode chamber should increase MFC power densities. Indeed, higher oxygen partial pressures, which increase oxygen reduction catalyst site occupancy, are routinely utilized for proton-exchange membrane fuel cells with hydrogen as the energy carrier (*18*).

Here, we studied the effect of a pressurized cathode chamber in an MFC on the power density by using an electrolyte cathode with an oxygen reduction catalyst configuration. In addition, the requirement of a membrane to prevent the crossover of oxygen from the pressurized cathode to the pressurized anaerobic anode was tested. We, therefore, chose a previously published MFC design with an upflow hydraulic pattern for which the ion-exchange membranes (AEM or CEM) could be exchanged or removed without disturbing the anode during a long-term operating period of

* Corresponding author phone: +1 (607) 255-2480; fax: +1 (607) 255-4080; e-mail: la249@cornell.edu.
[†] Washington University in St. Louis.
[‡] United States Department of Agriculture.
[§] Cornell University.

10.1021/es8015292 CCC: $40.75
Published on Web 10/15/2008

9 months (*19*). Steady anode operating conditions were necessary to isolate and study the effects of changing cathode conditions. Before removing the membrane, however, the effect of the anode effluent as the catholyte in place of the phosphate buffer solution was taken into consideration. For all conditions, supporting performance data was gathered for power generation (power density, current density, potential, and Coulombic efficiency) and waste treatment characterization (chemical oxygen demand [COD], volatile fatty acids [VFA], pH, and CH_4/CO_2 gas production).

Materials and Methods

Setup. The upflow MFC (UMFC) consisted of two chambers, an anaerobic anode chamber on the bottom (480 cm^3 total; 420 cm^3 net anode volume) and a cathode chamber (260 cm^3 total; 250 cm^3 net cathode volume) on the top (*19*). The anode electrode consisted of 8.0 m of carbon fiber (unsized fiber, Zoltek, St. Louis, MO) inserted randomly into the anode chamber. The cathode electrode was made of parallel sheets of carbon paper (AVCARB P75 carbon fiber paper, Ballard Material Products, Inc., Lowell, MA) (521 cm^2 total surface area) secured by carbon fiber (Zoltek) to the electrode external conductor (Supporting Information Figure S1). The cathode electrode was coated with 0.0189 mol/m^2 (3.65 g/m^2) of platinum (Pt) by chemical deposition of Pt with 0.976 mmol (0.4 g) chloroplatinic acid hexahydrate ($H_2PtCl_6 \cdot 6H_2O$) (Sigma-Aldrich), according to Gharibi et al. (*20*). The $H_2PtCl_6 \cdot 6H_2O$ was first dissolved in deionized water, followed by immersion of the carbon paper electrode in the solution. The solution was then ultrasonicated and heated to 80 °C. A sodium formate solution (40 g/L) (Sigma-Aldrich, St. Louis, MO) was added to the $H_2PtCl_6 \cdot 6H_2O$ solution, ultrasonicated, and heated for 1 h to reduce Pt. The carbon electrode was then removed and dried overnight at 105 °C. For experiments A−H (see the Experimental Design section), no Nafion coating was applied. Only prior to experiments I−K, two coatings of Nafion (5% solution) were applied to the cathode electrode to protect the Pt catalyst from the anolyte. Ion-exchange membranes consisted of either AEM or CEM (AMI-7001, CMI-7000 Membranes International, Glen Rock, NJ) (28.26 cm^2). The *anode* effluent line outlet was positioned 1.4 m above the ion-exchange membrane to maintain a 13.79 kPa back-pressure on the anode compartment. This anode back-pressure was designed to reduce the cathode to anode oxygen diffusion during operating periods with a pressurized cathode and should not adversely affect the microbial community (*21*). Anodic biogas production was measured with a gas meter (Ritter MGC-1 milligas counter, Bochum, Germany), and gas composition samples were taken through a septum that was placed after a liquid/gas separator located in the anode effluent tubing.

Cathode air pressure was increased by using a pressure regulator (Lowes Kobalt mini regulator, Mooresville, NC). Compressed air was continuously sparged through an air diffuser (Lee's, San Marcos, CA).

Operation. The inoculum was a homogenized granular sludge from an upflow anaerobic bioreactor at a brewery (Anheuser Busch, Inc., St. Louis, MO). The UMFC was fed a sucrose synthetic wastewater with a COD concentration of 900 mg/L and a continuous flow rate of 550 mL/day. The anode hydraulic retention time (HRT) was 18 h. The synthetic wastewater consisted of (per liter of deionized water): sucrose, 0.8 g; yeast extract (Difco Laboratories, Inc., Detroit, MI), 0.006 g; NH_4Cl, 0.033 g; K_2SO_4, 0.006 g; $FeCl_2 \cdot 4H_2O$, 0.033 g; iron citrate, 0.011 g; NaCl, 5.0 g; KCl, 0.1 g; $CaCl_2$, 0.1 g; $MgCl_2 \cdot 6H_2O$, 0.1 g; 0.040 M phosphate buffer; and trace elements, 1.0 mL modified from refs *22* and 23. The anolyte conductivity at 25 °C was 8.9 mS/cm. Anolyte was recirculated with a flow rate of 75 mL/min throughout the experiments. The anode temperature was maintained at 35 ± 1 °C with an external recirculation heater (Scientific model 1104 VWR, West Chester, PA). The cathode electrode was submersed in a 700 mM phosphate-buffered catholyte solution (Sigma-Aldrich, St. Louis, MO) and continuously replenished at a rate of 160 mL/day to maintain a constant pH level of 7.6 throughout the experiment with this catholyte. The catholyte conductivity at 25 °C was 124.5 mS/cm. Peristaltic pumps were used for both the anolyte recirculation and catholyte replenishment (Cole Parmer, Vernon Hills, IL). Sustainable fuel cell operating periods used a 100 Ω external resistor.

Analyses. The potential (E) across a resistor (R) was measured using a digital multimeter (2700 + 7700 multiplexer, Keithley Instruments, Inc., Cleveland, OH). The current density was calculated as $I = E/RV$, and the power density was calculated as $P = E^2/RV$, where V was the net liquid volume of the anode chamber. The polarization curve was developed by changing the external resistor stepwise from open circuit to 20 Ω. The internal (R_i) resistance was determined using the steady discharging method (*24*). Influent total COD, effluent soluble COD (SCOD), VFA, pH, and conductivity were measured according to procedures described in Standard Methods (*25*). For the conductivity measurements a self-contained conductivity meter was used (series 11, Oakton Instruments, Vernon Hills, IL). Gas analysis was performed with gas chromatography (Gow-Mac model 69-350, 4 in. × 1/8 in. o.d. 20% DC-200 on Chromosorb P AW-DMCS, 80/100 mesh column, Bethlehem, PA). All analyses were performed in triplicate with the exception of the biogas production and pH for which daily measurements were recorded.

The theoretical increase in the cathode potential with increasing air pressure was calculated with the Nernst equation. This equation was used in its simplified form because all other performance variables (temperature, feed rate, feed composition, recirculation rate, reactor configuration) were maintained constant with the exception of the pressure (*18*):

$$\Delta E = \frac{RT}{4F} \ln\left(\frac{P_2}{P_1}\right)$$

where E = potential, R = universal gas constant, T = temperature, F = Faraday's constant, and P_i = absolute cathode pressure.

Experimental Design. The study was conducted over a 9 month period of time, with the following experimental sequence: experiment A, 34.48 kPa with AEM; B, 17.24 kPa with AEM; C, nonreplenished catholyte pH test with AEM at 17.24 kPa (the continuous catholyte replenishment was temporarily switched off); D, atmospheric pressure with AEM; E, atmospheric pressure with CEM; F, 34.38 kPa with CEM; G, 17.24 kPa with CEM; H, nonreplenished catholyte pH test with CEM at 17.24 kPa (the continuous catholyte replenishment was temporarily switched off); I, atmospheric pressure with Nafion-coated cathode with CEM and phosphate-buffered catalyst; J, atmospheric pressure with Nafion-coated cathode with CEM and anolyte effluent as catholyte; K, atmospheric pressure without a membrane and with the anode effluent flowing from the anode to the cathode in an upward mode (Supporting Information Figure S2). The recirculation of the anolyte was sustained during experiments J and K.

Results and Discussion

Pressurized Cathode Chamber Increases MFC Power Densities. The highest power density of our study (7.29 W/m^3) was achieved with 17.24 kPa of cathode pressure and an AEM (Figure 1 and Table 1). The power density at a 17.24 kPa pressure represented a 70% and 13% improvement in comparison to atmospheric pressure and 34.48 kPa, respec-

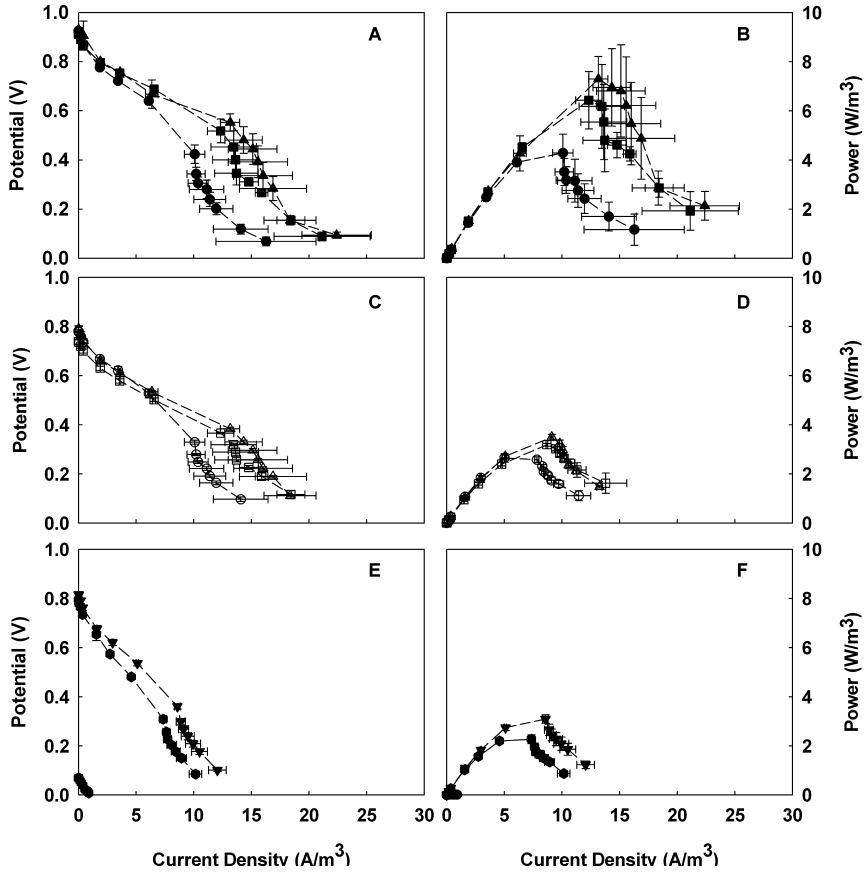

FIGURE 1. UMFC polarization and power curves: (A) polarization curve with AEM; (B) power curve with AEM; AEM data are represented with solid symbols, (■) 34.48 kPa, (▲) 17.24 kPa, and (●) atmospheric pressure; (C) polarization curve with CEM; (D) power curve with CEM; CEM data are shown with hollow symbols, (□) 34.48 kPa, (Δ) 17.24 kPa, and (○) atmospheric pressure; (E) polarization curve with atmospheric pressure cathode, (▼) Nafion-coated cathode electrode with phosphate-buffered catholyte, (⬣) Nafion-coated cathode with anolyte effluent catholyte, and (●) membrane removed; (F) power curve with atmospheric pressure cathode, (▼) Nafion-coated cathode electrode with phosphate-buffered catholyte, (⬣) Nafion-coated cathode with anolyte effluent catholyte, and (●) membrane removed. Data points represent an average of three polarization curves with the accompanying standard deviation error bars (presented as a color image in Supporting Information Figure S5).

TABLE 1. UMFC Electrical Performance Data

experiment	cathode air pressure (kPa)	exchange membrane	OCP (mV)[a]	max power density (W/m³)[a]	max current density (A/m³)[a]	potential at 100 Ω (mV)[a]	Coulombic efficiency (%)[b]
A	34.48	AEM	913 (2)	6.43 (1.17)	12.34 (1.15)	518 (48)	7.9
B	17.24	AEM	931 (9)	7.29 (0.93)	13.16 (0.83)	553 (35)	8.6
D	atm	AEM	925 (6)	4.29 (0.77)	10.07 (0.89)	423 (37)	6.8
F	34.48	CEM	737 (9)	3.18 (0.06)	8.70 (0.08)	366 (3)	5.4
G	17.24	CEM	790 (12)	3.49 (0.12)	9.12 (0.13)	383 (7)	6.3
E	atm	CEM	780 (6)	2.58 (0.12)	7.83 (0.18)	329 (8)	3.6
I	atm	CEM-NC[c]	816 (11)	3.09 (0.17)	8.57 (0.11)	360 (10)	6.5
J	atm	CEM-AC[d]	795 (2)	2.27 (0.18)	7.35 (0.29)	309 (12)	3.8
K	atm	none	70 (13)	0.01	0.37 (0.03)	23 (1)	0.2

[a] Single standard deviations noted in parenthesis. [b] Coulombic efficiency calculated with average maximum current density and average COD removal data. [c] NC—Nafion-coated cathode electrode. [d] AC—anolyte to cathode configuration.

tively (experiments B, D, and A). Further, the fuel cell open circuit potential (OCP) at 17.24 kPa with the AEM was 0.931 V, and this is to our knowledge the highest recorded for a platinum oxygen-reducing cathode in an MFC (Figure 1A and Table 1). As anticipated, the cathode potential increased with increasing air pressure, reflecting the increasing catholyte dissolved oxygen concentrations (Supporting Information Table S1). The cathode OCP (vs Ag/AgCl, sat. KCL, 0.195 V vs standard hydrogen electrode [SHE]) was 0.3059, 0.3261, and 0.3545 V for atmospheric pressure, 17.24, and 34.48 kPa, respectively (Supporting Information Figure S3). With CEM, the highest power density (3.49 W/m³) also occurred at 17.24 kPa compared to atmospheric pressure and 34.48 kPa (Figure 1D and Table 1) (experiments G, E, and F). The power density with the 17.24 kPa cathode pressure represented a 35% and 10% improvement compared to atmospheric pressure and 34.48 kPa, respectively.

We predicted with the Nernst equation that an increase in pressure from atmospheric pressure to 17.24 and 34.48 kPa would increase the cathode cell potential by 0.0010 and 0.0019 V, respectively. However, our experimental data showed higher than predicted cathode potential increases

of 0.0202 and 0.0468 V for 17.24 and 34.48 kPa, which represents a 20- and 25-fold increase over the Nernst equation predicted potentials, respectively. The difference in actual versus predicted potentials was explained for fuel cells by a decrease in the irreversible activation losses at the cathode electrode, especially at lower temperatures (*18*). The decrease in the cathode electrode's irreversible activation losses is related to the exchange current density, which refers to the steady-state forward and backward flow of electrons between reactants and products at the electrode surface. With an increase in the oxygen partial pressure, the exchange current density increased, reflecting a more active cathode electron flux. The more active cathode requires a lower overpotential to energize cathode electron-transfer reactions. Thus, increasing exchange current density (by increasing the oxygen partial pressure, increasing the cathode temperature, or by using more effective cathode catalysts) lowers the irreversible activation losses required to energize chemical reactions (*18*).

We anticipated increasing MFC power densities with increasing cathode pressure. Our data, however, showed that power densities decreased as the cathode pressure was increased from 17.24 to 34.48 kPa. At 100 Ω of external resistance, the cathode potential increased from 141 to 179 mV (Supporting Information Figure S3) and the corresponding MFC potentials decreased from 553 to 518 mV (Table 1) when the pressure was increased from 17.24 to 34.48 kPa. The differences between the cathode and MFC potentials indirectly indicate an anode potential of −412 and −339 mV for 17.24 and 34.48 kPa, respectively. We believe that the lower anode potential (−339 mV) is most likely the result of increased oxygen crossover through the ion-exchange membrane at higher pressures. We found experimentally that oxygen diffusion increased with increasing differential pressures across the membrane (Supporting Information Figure S4), supporting the theory that oxygen diffusion at the highest cathode pressure (34.48 kPa) negatively impacted performance. A similar phenomenon of lower overall cell potentials at a higher cathode potential was found in a sediment fuel cell study that used a rotating cathode. The cathode potential was improved by increasing the speed of cathode rotation; however, the overall fuel cell potential declined because of the increased oxygen concentrations in the sediment (*26*). Since diffusion of oxygen over the ionic membrane is affected by both oxygen concentration and pressure gradients, a back-pressure on the anode compartment was utilized to minimize oxygen diffusion from the cathode to the anode. The negative effect of the oxygen diffusion at 17.24 kPa was reduced because of a 13.79 kPa back-pressure on the anode chamber and a resulting catholyte to anolyte pressure gradient of only 3.45 kPa. This pressure gradient increased to 20.69 kPa with the 34.48 kPa cathode, thereby increasing the oxygen diffusion. Our data, thus, suggest that equalizing and optimizing the pressures in the cathode and anode chambers can further increase the overall cell potential and power densities.

Anolyte Effluent as Catholyte and Membraneless Operation Reduce MFC Power Densities. Three additional experiments were conducted with an atmospheric pressure cathode and a 13.79 kPa anode (constant back-pressure throughout the entire experimental period): (1) a baseline experiment with a CEM and phosphate-buffered catholyte (experiment I), (2) CEM and anolyte effluent (experiment J), and (3) the removal of CEM (experiment K). We observed a 26.5% decrease in the power density with the change from the phosphate-buffered catholyte (experiment I) to the anode effluent catholyte (experiment J) because of immediate and longer term effects, which are discussed in detail in the Supporting Information. In addition, operation without a membrane (experiment K) resulted in a 99.5% decrease in the power density compared

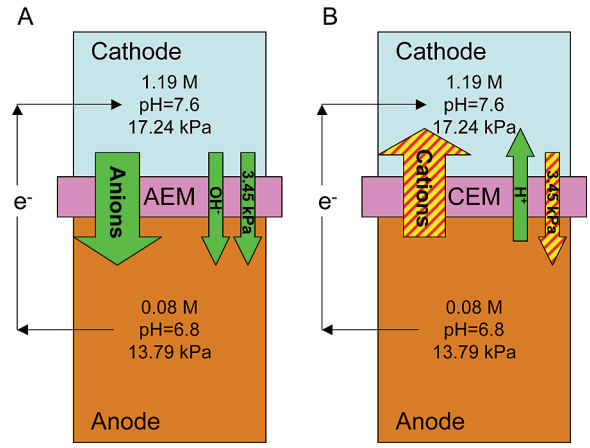

FIGURE 2. UMFC monovalent ion charge equivalents and ion transport: monovalent charge equivalents (cation, anion, proton, and hydroxide ions) and hydraulic pressures are illustrated for the UMFC during experiments B and G. The direction, size, and shading of the arrows reflect the dominant ion transport mechanisms to achieve fuel cell electroneutralilty: (A) electroneutrality maintenance with the AEM requires the movement of negatively charged ions from the cathode to the anode. The large downward anion arrow represents the favorable transport of anions with the concentration gradient, and (B) electroneutrality maintenance with the CEM requires the movement of positively charged ions from the anode to the cathode. The large upward cation arrow is cross-hatched because cation transport was moving against the ion concentration gradient. The pressure gradients were less important (smaller arrow) and were a driving force for AEM or a restraint (cross-hatched) for CEM to move ions across the membrane. Proton and hydroxide ion gradients were equivalent for both membranes and are much less important at neutral pH levels (smaller arrows).

to experiment J with CEM and anolyte effluent as catholyte (0.01 vs 3.09 W/m^3) and 99.6% to the baseline experiment I (Table 1), which strongly suggests that removing the ion-exchange membrane in an MFC with an electrolyte cathode and oxygen reduction catalyst severely deteriorates the power density due to oxygen crossover, cathode insulation, and/or catalyst poisoning (see the discussion in the Supporting Information).

Ion Gradients Influence Internal Resistance and Power Densities. With ion transport being imperative to maintain electroneutrality, ohmic losses become important because they contribute to MFC total system losses. Ohmic losses in MFCs are influenced by the (1) ionic transport processes within the anolyte and catholyte (i.e., solution losses due to diffusion and electromigration processes) (*10*−*12*) and (2) ionic transport processes across the exchange membrane (i.e., membrane losses due to the specific material features of the membrane and characteristics of the electrolyte solutions) (*27*). Our UMFC had concentration and hydraulic pressure gradients over the ion-exchange membrane (because of different anolyte and catholyte solutions and operating conditions, see Figure 2), which can be either a driving force or restraint for ion movement from one compartment to the other. We maintained identical ion and hydraulic pressure gradients with constant anolyte and catholyte solutions (i.e., 0.08 and 1.19 M monovalent equivalents, respectively) during the comparison experiments with AEM and CEM, and thus we anticipate similar solution losses. Kim et al. (*27*) found comparable internal resistances for the same AEM and CEM materials without ion gradients across the membranes. Therefore, since the solution losses and specific material membrane losses were similar between AEM and CEM experiments, we anticipate different membrane losses due to the impact of the ion gradient and to a

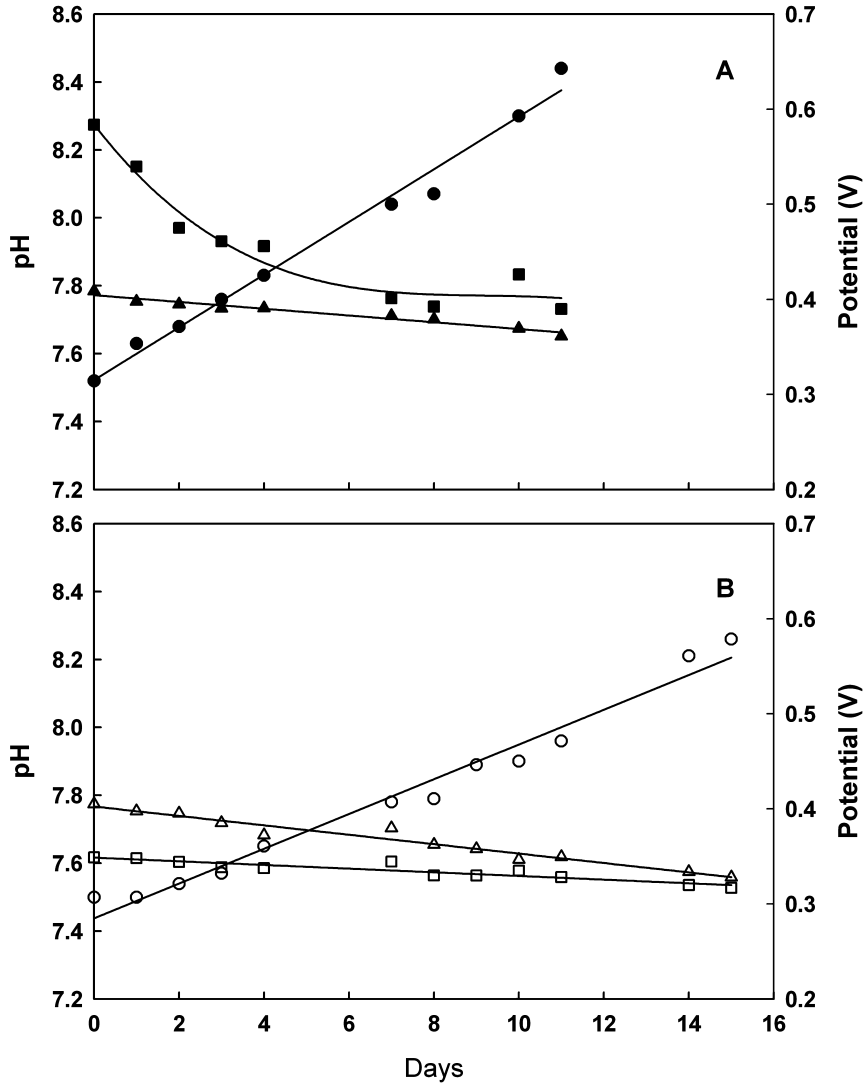

FIGURE 3. pH trends, cathode potentials, and overall cell potentials with nonreplenished phosphate-buffered catholyte: (A) AEM data for experiment C represented with solid symbols and (B) CEM data for experiment H represented with hollow symbols. Squares (■ AEM; □ CEM) indicate the overall potential across the fuel cell, triangles (▲ AEM; Δ CEM) indicate the cathode potential, and circles (● AEM; ○, CEM) the catholyte pH.

lesser extent (due to a modest 3.45 kPa pressure differential) the hydraulic pressure gradient: the choice of AEM versus CEM will dictate whether anions or cations, respectively, travel selectively across the ion-exchange membrane to maintain fuel cell electroneutrality (*10*−*12*). In our study with AEM, anion transport was favorable *with* the concentration and hydraulic pressure gradients (Figure 2A), whereas with CEM cations (non-protons) were transported *against* the concentration and hydraulic pressure gradients (Figure 2B). Thus, a favorable ion gradient will result in lower membrane losses compared to a nonfavorable ion gradient.

Indeed, our results consistently yielded higher power densities for the AEM compared to the CEM (Figure 1, parts A and C, and Table 1). More specifically for experiments B and G with 17.24 kPa, a lower internal resistance of 61.2 Ω for AEM compared to 93.6 Ω for CEM was estimated. As explained above, the favorable anion versus the nonfavorable cation gradient in our study accounts for the ~30 Ω difference in internal resistance. This quantitative difference was caused by our choice of composition and concentration of phosphate buffer solution in the cathode chamber and would have been less pronounced if we had used a lower concentration phosphate solution in the cathode. In a real-world situation, the ion gradients between the anode and cathodes are dependent on the encountered wastewater solution (anolyte) and selected catholyte. On the basis of these solutions the engineer should decide between AEM and CEM to minimize the overall MFC resistance.

Monovalent Ions Show Lower Charge-Transfer Resistance than Divalent Ions. Measurement of catholyte pH trends with a nonreplenished phosphate-buffered catholyte (experiments C and H) showed an anticipated increase in pH levels over time for both the AEM and CEM (at 17.24 kPa) (Figure 3). Such increases in pH reflect proton-consuming oxygen reduction reactions in the cathode (whereas hydroxide ions and protons do not transfer to maintain electroneutrality). The slightly greater pH increase for the AEM compared to the CEM was accounted for by the higher current densities with the AEM (Figure 3A). Cathode potential for both AEM and CEM over time during batch operating conditions showed a slow decrease as the pH increased, which follows the Nernst equation (0.34 mV/pH AEM; 0.69 mV/pH CEM measured vs 0.59 mV/pH predicted). The overall cell potential profiles for the UMFC with AEM and CEM, however, differed considerably from each other. The cell potential decline with the AEM was initially rapid and then approximated the cathode potential decrease (Figure 3A). With the CEM, however, the cell potential decline continually corresponded with the decrease in the cathode potential (Figure 3B). The difference in the cell potential profiles could

TABLE 2. UMFC Wastewater Treatment Data

experiment	cathode air pressure (kPa)	exchange membrane	% COD removal[a]	effluent VFA (mg/L)[a]	cm^3 gas/mg COD feed	effluent gas composition $\%CH_4/\%CO_2$
A	34.48	AEM	93.7 (0.7)	38.5 (8.1)	0.109	NA
B	17.24	AEM	95.2 (0.8)	73.9 (3.2)	0.085	NA
D	atm	AEM	93.6 (3.0)	48.5 (14.2)	0.091	NA
F	34.48	CEM	97.6 (0.7)	50.4 (26.3)	0.147	77.2/8.6
G	17.24	CEM	93.1 (6.3)	46.9 (0.0)	0.172	71.6/8.8
E	atm	CEM	96.4 (13.8)	55.3 (23.8)	0.097	73.1/8.0
I	atm	CEM-NC[b]	NA	47.9 (21.2)	0.013	73.0/8.0
J	atm	CEM-AC[c]	97.7 (1.8)	18.7 (7.5)	0.008	70.7/7.5
K	atm	none	93.8 (2.7)	25.4 (11.9)	0.001	NA

[a] Single standard deviations noted in parenthesis. [b] NC—Nafion-coated cathode electrode. [c] AC—anolyte to cathode configuration.

not be attributed to the pH, cathode potential, or the initial ion concentrations because these variables were similar for the AEM and CEM experiments. Therefore, we hypothesized that ionic transport processes across the exchange membrane were influencing the cell potential. Indeed, we could explain the difference in cell potential profiles by a preferential transfer of monovalent versus divalent ions crossing the membrane due to the smaller radius of the monovalent ion compared to the divalent ion. The pH increase from 7.5 to 8.2 in the nonreplenished cathode greatly influenced the equilibrium of monovalent ($H_2PO_4^-$) and divalent (HPO_4^{2-}) phosphate ions (the monovalent/divalent ratio decreased from 0.35 to 0.07 based on the acid/base equilibrium). The resulting increase in the concentration of divalent phosphate ions coincided with the rapid decrease in the MFC potential with AEM. This indicates increasing resistance losses with the membrane transfer of divalent anions compared to monovalent anions because of the larger radius of the divalent phosphate ions in comparison to the monovalent. The number of tightly bound water molecules that move with the ion as it diffuses is 1.91 and 3.95 for the monovalent and divalent phosphate ions, respectively, resulting in equivalent hydrated sphere radius of 3.02 and 3.27 Å (*28*). This observation is supported by Rozendal et al. (*12*), who measured cation transport across a Nafion 117 membrane to maintain electroneutrality and also found that the monovalent cations (Na^+, K^+, and NH_4^+) transferred more readily than the divalent cations (Ca^{2+} and Mg^{2+}). This selectivity of monovalent versus divalent ions reflects the differences in equivalent hydration radius of these ions (*28*). For the CEM, cation transport from the anode to cathode is required to maintain fuel cell electroneutrality. Whereas the nonreplenished cathode had a changing pH, the anode, which was replenished, had a stable pH in these experiments. Thus, the monovalent to divalent cation equilibrium for the anolyte in the UMFC with CEM ion transport was constant because the anode chamber was continuously replenished, resulting in an overall cell potential decrease that closely matched the decrease in the cathode potential (Figure 3).

Wastewater Treatment. The COD removal rates with UMFC treatment were high (93.1−97.7%) regardless of cathode pressure, type of membrane, or the presence/absence of a membrane (Table 2). Relatively low Coulombic efficiencies (3.6−8.6% in Table 1) indicate that electricigens were not the primary COD-consuming microbes in the UMFC. Instead, methanogens were the primary COD removing microbes indicated by a methane content of 70% in the off gas from the anode chamber. Other factors that contributed to the high COD removals were the presence of facultative anaerobes utilizing the oxygen that diffused through the ion-exchange membranes at higher cathode air pressures and the accumulation of biomass due to cellular growth. As anticipated, Coulombic efficiencies positively correlated with power densities and MFC potential at 100 Ω of external resistance (Table 1). The relatively low Coulombic efficiencies indicate that this work was performed with a nonoptimized MFC for research purposes. This design was chosen because the membrane had to be replaced or removed without disturbing the anode. Similar relative increases in overall power densities are anticipated with a more optimized design, and for example, an anticipated potential increase from 0.4 to 0.5 V at 10 Ω resistance will increase the power density by 25% based on Ohm's law. However, many questions remain for future MFC research before implementation as a wastewater treatment device: Are the gains in MFC power densities economical considering the energy required to pressurize air? What is the optimum cathode pressure? Are there effective cathode and anode pressure balancing designs that will enable the benefits of higher cathode air pressures while minimizing the negative effects of oxygen diffusion? Can catholyte composition and ion gradients be designed to minimize ohmic resistance? The knowledge gained from this study, and addressing the above questions, will help advance MFC design, potentially leading to more sustainable wastewater treatment processes.

Acknowledgments

The financial support for this work was provided through a specific collaborative agreement between Washington University in St. Louis and the Fermentation Biotechnology Research Unit, USDA, Agricultural Research Service, Peoria, Illinois and the National Science Foundation through Grant No. 0645021. We thank Sarah Dryden and anonymous reviewers for critically evaluating the manuscript.

Supporting Information Available

Additional information on the materials and methods, figures showing the UMFC cathode electrode assembly, the UMFC process flow with and without ion-exchange membrane, the cathode potential versus current density, the membrane oxygen diffusion at different pressures, and the UMFC polarization and power curves, and a table containing dissolved oxygen concentration data. This material is available free of charge via the Internet at http://pubs.acs.org.

Literature Cited

(1) Burton, F. L. Water and wastewater industries: Characteristics and energy management opportunities; Electric Power Research Institute, Inc. (EPRI), Community Environmental Center: St. Louis, MO, 1996.

(2) Logan, B. E. Biologically extracting energy from wastewater; biohydrogen production and microbial fuel cells. *Environ. Sci. Technol.* **2004**, *38,* 160A–167A.

(3) Liu, H.; Logan, B. E. Electricity generation using an air-cathode single chamber microbial fuel cell in the presence and absence of a proton exchange membrane. *Environ. Sci. Technol.* **2004**, *38*, 4040–4046.
(4) Rabaey, K.; Lissens, G.; Siciliano, S. D.; Verstraete, W. A microbial fuel cell capable of converting glucose to electricity at high rate and efficiency. *Biotechnol. Lett.* **2003**, *25*, 1531–1535.
(5) Rabaey, K.; Verstraete, W. Microbial fuel cells: Novel biotechnology for energy generation. *Trends Biotechnol.* **2005**, *23*, 291–298.
(6) Clauwaert, P.; Van der Ha, D.; Boon, N.; Verbeken, K.; Verhaege, M.; Rabaey, K.; Verstraete, W. Open air biocathode enables effective electricity generation with microbial fuel cells. *Environ. Sci. Technol.* **2007**, *41*, 7564–7569.
(7) Rabaey, K.; Clauwaert, P.; Aelterman, P.; Verstraete, W. Tubular microbial fuel cells for efficient electricity generation. *Environ. Sci. Technol.* **2005**, *39*, 8077–8082.
(8) Logan, B.; Cheng, S.; Watson, V.; Estadt, G. Graphite fiber brush anodes for increased power production in air-cathode microbial fuel cells. *Environ. Sci. Technol.* **2007**, *41*, 3341–3346.
(9) He, Z.; Wagner, N.; Minteer, S. D.; Angenent, L. T. The upflow microbial fuel cell with an interior cathode: Assessment of the internal resistance by impedance spectroscopy. *Environ. Sci. Technol.* **2006**, *40*, 5212–5217.
(10) Zhao, F.; Hamisch, F.; Schroder, U.; Scholz, F.; Bogdanoff, P.; Hermann, I. Challenges and constraints of using oxygen cathodes in microbial fuel cells. *Environ. Sci. Technol.* **2006**, *40*, 5193–5199.
(11) Harnisch, F.; Schröder, U.; Scholz, F. The suitability of monopolar and bipolar ion exchange membranes as separators for biological fuel cells. *Environ. Sci. Technol.* **2008**, *42*, 1740–1746.
(12) Rozendal, R. A.; Hamelers, H. V. M.; Buisman, C. J. N. Effects of membrane cation transport on pH and microbial fuel cell performance. *Environ. Sci. Technol.* **2006**, *40*, 5206–5211.
(13) Min, B.; Kim, J.; Oh, S.; Regan, J. M.; Logan, B. E. Electricity generation from swine wastewater using microbial fuel cells. *Water Res.* **2005**, *39*, 4961–4968.
(14) Liu, H.; Ramnarayanan, R.; Logan, B. E. Production of electricity during wastewater treatment using a single chamber microbial fuel cell. *Environ. Sci. Technol.* **2004**, *38*, 228–225.
(15) Feng, Y.; Wang, X.; Logan, B. E.; Lee, H. Brewery wastewater treatment using air-cathode microbial fuel cells. *Appl. Microbiol. Biotechnol.* **2008**, *78*, 873–880.
(16) He, Z.; Angenent, L. T. Application of bacterial biocathodes in microbial fuel cells. *Electroanalysis* **2006**, *18*, 2009–2015.
(17) Rozendal, R. A.; Jeremiasse, A. W.; Hamelers, H. V.; Buisman, C. J. Hydrogen production with a microbial biocathode. *Environ. Sci. Technol.* **2008**, *42*, 629–634.
(18) Larminie, J.; Dicks, A. *Fuel Cell Systems Explained*, 2nd ed.; John Wiley & Sons, Ltd.: Chisester, West Sussex, England, 2003.
(19) He, Z.; Minteer, S. D.; Angenent, L. T. Electricity generation from artificial wastewater with an upflow microbial fuel cell. *Environ. Sci. Technol.* **2005**, *39*, 5262–5267.
(20) Gharibi, H.; Mirzaie, R. A.; Shams, E.; Zhiani, M.; Khairmand, M. Preparation of platinum electrocatalysts using carbon supports for oxygen reduction at a gas-diffusion electrode. *J. Power Sources* **2005**, *139*, 61–66.
(21) Wood, E. J. F. *Marine Microbial Ecology*; Reinhold Publishing Company: New York, 1965.
(22) Angenent, L. T.; Sung, S. Development of anaerobic migrating blanket reactor (AMBR), a novel anaerobic treatment system. *Water Res.* **2001**, *35*, 1739–1747.
(23) Zehnder, A. J. B.; Huser, B. A.; Brock, T. D.; Wuhrmann, K. Characterization of an acetate-decarboxylating, non-hydrogen-oxidizing methane bacterium. *Arch. Microbiol.* **1980**, *124*, 1–11.
(24) Liang, P.; Huang, X.; Fan, M. Z.; Cao, X. X.; Wang, C. Composition and distribution of internal resistance in three types of microbial fuel cells. *Appl. Microbiol. Biotechnol.* **2007**, *77*, 551–558.
(25) Clesceri, L. S.; Greenberg, A. E.; Eaton, A. D. *Standard Methods for the Examination of Water and Wastewater*, 20th ed.; American Public Health Association: Washington, DC, 1998.
(26) He, Z.; Shao, H.; Angenent, L. T. Increased power production from a sediment microbial fuel cell with a rotating cathode. *Biosens. Bioelectron.* **2007**, *22*, 3252–3255.
(27) Kim, J. R.; Cheng, S.; Oh, S. E.; Logan, B. E. Power generation using different cation, anion, and ultrafiltration membranes in microbial fuel cells. *Environ. Sci. Technol.* **2007**, *41*, 1004–1009.
(28) Kiriukhin, M. Y.; Collins, K. D. Dynamic hydration numbers for biologically important ions. *Biophys. Chem.* **2002**, *99*, 155–168.

ES8015292